Article:
Zhang, B., Ge, C., Xu, X. et al. (4 more authors) (2025) Evolution mechanism of wear characteristics of cylinder liner and piston ring under starved lubrication condition. Tribology International, 208. 110622. ISSN: 0301-679X

https://doi.org/10.1016/j.triboint.2025.110622

Evolution mechanism of wear characteristics of cylinder liner and piston ring under starved lubrication condition

Baofeng Zhang[1], Chang Ge[1], Xing Xu[1], Lining Liu[2], Xuan Ma[1*], Ardian Morina[3], Xiqun Lu[1*]

1. College of Power and Energy Engineering, Harbin Engineering University, Harbin, China;
2. College of Mechanical and Electrical Engineering, Harbin Engineering University, Harbin, China;
3. School of Mechanical Engineering, University of Leeds, Leeds, UK;

Corresponding authors: Xuan Ma, Associate professor;

E-mail: maxuan@hrbeu.edu.cn

Xiqun Lu, Professor;

E-mail: luxiqun@hrbeu.edu.cn

Highlights:

- The evolution process of the cylinder liner wear state is reproduced by designing a starved lubrication sliding wear test.
- The mechanism of cylinder liner scuffing under the condition of starved lubrication is revealed.
- The effect of the microstructure of cylinder liner material on the wear process is analyzed.
- The function and failure mechanism of the tribo-layer in the wear process are analyzed.

Evolution mechanism of wear characteristics of cylinder liner and piston ring under starved lubrication condition

Abstract： This study conducted high-temperature sliding wear tests on cylinder liners and piston rings under starved lubrication conditions, using a step-loading method to analyze the wear state transition of the cylinder liner. Surface and interface characteristics under various wear conditions were examined through optical microscopy (OM), white light interferometry, scanning electron microscopy (SEM), and transmission electron microscopy (TEM), and the mechanism of wear state transition was explored. The results indicate that the friction coefficient initially increases, then decreases, and increases again with rising load. The initial increase is attributed to the formation of a local tribo-layer and increased surface roughness. As the tribo-layer expands in area and thickness, the friction coefficient gradually decreases. However, with further load increase, the tribo-layer begins to wear down until scuffing occurs, leading to a rapid rise in the friction coefficient. Graphite and phosphorus eutectic in the cylinder liner are primary contributors to crack formation in the tribo-layer and substrate. Additionally, the tribofilm formed on the initial wear scar surface further contributes to crack formation.

Keywords： Cylinder liner piston ring， Wear state transition， Tribo-layer， Scuffing

1. Introduction

As a crucial friction pair in internal combustion engines, the primary function of the cylinder liner and piston ring is to form a sealed combustion chamber with the piston and cylinder head, converting the chemical energy from fuel combustion into mechanical energy. Wear between the cylinder liner and piston ring reduces the airtightness of the combustion chamber, increases fuel consumption, decreases thermal efficiency, and generates significant pollutant emissions [1, 2]. Under harsh working conditions, this wear can lead to scratching, scuffing, and even seizure between the cylinder liner and piston ring [3, 4]， directly impacting engine reliability and service life. Therefore, understanding the wear process of cylinder liners and piston rings under different conditions holds significant engineering importance.

Previous studies have identified several key wear mechanisms between cylinder liners and piston rings, including abrasive wear, oxidative wear, fatigue wear, and scuffing wear [5-9]. Each wear mechanism results in distinct wear behaviors. For instance, abrasive and oxidative wear tend to have low wear rates and are generally unavoidable during engine operation. In contrast, fatigue wear and scuffing are severe, abnormal wear modes. Once this occurs, it can lead to the failure of either the cylinder liner or the piston ring [10, 11]. These forms of wear are especially prevalent under harsh conditions and starved lubrication. For example, when the piston ring reaches the top dead center (TDC) of the cylinder liner, low speed, high pressure, and elevated temperatures hinder the formation of an effective lubricating oil film, leading to starved lubrication or dry friction, resulting in severe wear. The transition from mild wear to scuffing in the cylinder liner is influenced by various factors, with load being a primary one. Kamps et al. [12] replicated the process of transitioning from mild wear to scuffing in an engine through linear loading. Similarly, Olander et al. [6] tested the anti-scuffing performance of engine materials by gradually increasing the load. Temperature is another critical factor influencing scuffing. Walker et al. [13] examined the scuffing process of cylinder liner cast iron under dynamic loads using a linear heating method, finding that scuffing is temperature-dependent. Dahdah et al. [3] also concluded that the temperature gradient generated by the contact between the piston ring and cylinder liner is a key cause of scuffing. Contact friction-induced temperature changes cause the local lubricating oil film to rupture, leading to direct asperity contact. Moreover, temperature changes can lead to lubricant desorption, further contributing to asperity contact [14]. Besides temperature, material composition [15-17]， piston ring coatings [6, 18, 19], and lubricant properties [20-22] also play significant roles in scuffing occurrence. Although previous research has comprehensively analyzed the conditions that cause scuffing between the cylinder liner and piston ring, the scuffing process and its underlying mechanism under actual working conditions remain insufficiently explored.

Scuffing is a catastrophic form of abnormal wear, often resulting in rapid surface damage, loss of functionality, and integrity, accompanied by high wear rates and increased friction coefficients. Unlike other forms of wear, scuffing occurs suddenly

without prior signs [23, 24]. Two primary mechanisms are proposed to explain scuffing: one suggests that temperature is the main cause, where high contact flash temperatures break the lubricating oil film, leading to asperity welding as surfaces transition from solid to liquid [25, 26]. The rupture of the oil film is influenced by not only temperature but also load and speed. At low sliding speeds and high loads, boundary films are more prone to damage, resulting in scuffing [27]. The second mechanism links scuffing to the rupture of the tribo-layer or oxide layer on the contact surface. The breakdown of the oil film is a prerequisite for scuffing, but the actual surface damage is due to material transfer from the substrate. Typically, the friction surface of steel materials forms a thick, hard layer (or glaze layer), which prevents direct contact between the substrate materials and thus inhibits scuffing [28-30]. Several studies have reported on this hard layer. Saeidi et al. [31] investigated scuffing between cast iron and steel and found that the tribo-layer mainly consists of Fe_2O_3, with the reduction of Fe_2O_3 to α-Fe during friction causing scuffing. Jensen et al. [11] studied the cylinder scuffing process, identifying four distinct regions within the tribo-layer: the mechanical mixing layer, the fine-grained layer, the coarse-grained layer, and the substrate. Gussmagg et al. [7] experimentally replicated the scuffing process of cylinder liners and concluded that the tribofilm plays a key role in preventing scuffing between the piston ring and cylinder liner. However, observation of the surface morphology of the wear scars indicates that in addition to the tribofilm, there may also be an oxide layer present. The author also discovered a nanocrystalline layer of iron oxide during dry friction tests, which was used to investigate the wear behavior of the cylinder liner cast iron's microstructure. The detachment of this layer frequently results in scuffing [32]. From these reports, it is clear that while extensive studies have been conducted on scuffing, forming a unified conclusion remains challenging due to differences in research subjects, methods, and objectives.

In this study, the cylinder liner and piston ring were selected as the research objects, and a variable load test under starved lubrication conditions was used to simulate the wear state changes of the cylinder liner and the scuffing process. The stopping point of the test was determined by changes in the friction coefficient. By analyzing the microstructure and surface interface characteristics of the cylinder liner at different

stages, the wear transformation process of the cylinder liner was reproduced. This study reveals the evolution mechanism of the cylinder liner's surface interface under starved lubrication, providing a theoretical basis for wear evaluation and life prediction of cylinder liners.

2. Test procedure

2.1 Test materials

The cylinder liner and piston ring samples were sourced from an actual engine. The cylinder liner was made of gray cast iron, while the piston ring was made of ductile cast iron, with an amorphous Cr-C-Al alloy coating on the surface. The contact area's surface roughness was Ra ≤ 0.03. Fig. 1 shows the microstructure of the cylinder liner and piston ring materials. The cylinder liner was cut into a cuboid measuring 30 × 10 × 6 mm using an electric spark wire cutting machine, and the piston ring was processed into a 15 mm ring section. To clearly observe microstructural changes during the wear process, the cylinder liner sample was ground and polished to achieve a surface roughness of Ra ≤ 0.2. Full-formula engine lubricating oil with a viscosity grade of 15W-40 was used for lubrication during the test.

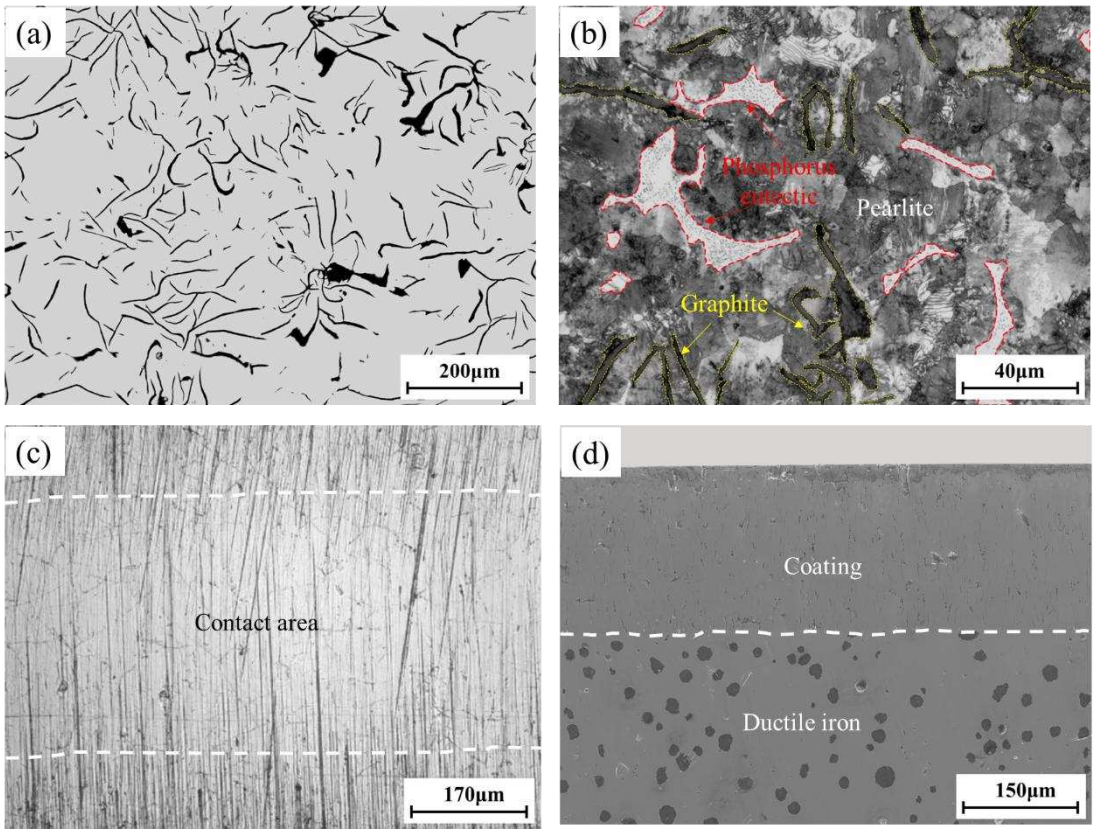

Fig. 1. Morphology and microstructure of cylinder liner and piston ring: (a) graphite morphology of cylinder liner, (b) microstructure of cylinder liner material, (c) contact surface morphology of piston ring, (d) cross-section morphology of piston ring.

2.2 Test parameter design

To prevent eccentric wear between the cylinder liner and piston ring during the test, and to better analyze the microstructural changes at the surface and interface during wear, the surface of the cylinder liner sample was ground and polished to eliminate the influence of surface morphology. The initial test load was set at 50 N, and a step-loading method was applied. As shown in Fig. 2, the load was increased by 50 N at each stage, with a runtime of 30 minutes per stage. Based on test results and relevant literature, scuffing between the cylinder liner and piston ring occurs when the coefficient of friction (Cof) exceeds 0.2 [7, 33]. Therefore, the test was set to automatically stop when the friction coefficient reached 0.3. During the test, the sliding frequency between the cylinder liner and piston ring sample was 2 Hz, with a sliding stroke of 20 mm, resulting in an average sliding speed of 0.08 m/s. The test was conducted under starved lubrication conditions. At the start of the test, 0.04 ml of lubricating oil was applied to the sample surface, and no additional oil was added until the end of the test. The average operating temperature range of the cylinder wall in an engine is approximately 90-120℃[5, 34]. To simulate actual engine conditions, the test temperature was set at 90℃.

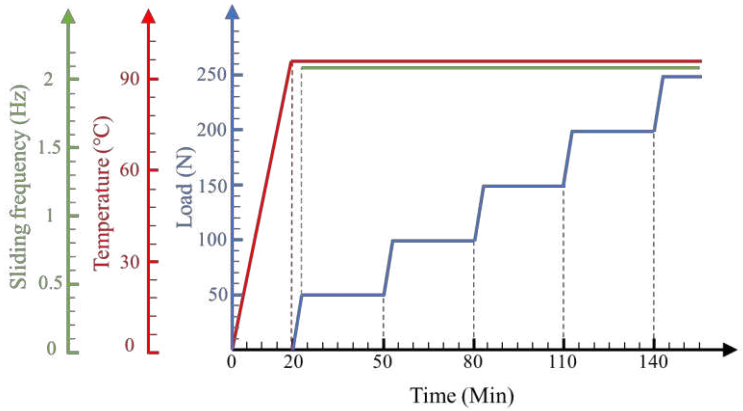

Fig. 2. Schematic diagram of parameter setting in the process of segmented loading test.

2.3 Wear test procedure

The lubricating oil consumption method is commonly used in the design of starved

lubrication tests. This method involves adding a specific amount of lubricating oil at the beginning of the test, which is gradually consumed as the test progresses until the end [31, 35]. In this study, the lubricating oil consumption method was employed to design the starved lubrication conditions. Before the test, the cylinder liner and piston ring samples were ultrasonically cleaned with anhydrous ethanol for 5 minutes to remove any residual oil from the surface. A syringe with a measuring scale was used to dispense 0.04 ml of lubricating oil onto the sample. The oil was then evenly spread across the surface using a rubber plate, forming a uniform oil film with a thickness of approximately 0.13 mm (Fig. 3). For details on the sample installation method and testing principle, please refer to previously published relevant work [32].

The sliding wear test was conducted on a multi-function tribology testing machine (MFT5000, Rtec Instruments), which is capable of automatically performing segmented loading and setting stop conditions based on either load or friction coefficient in its control program. To analyze the scuffing evolution process of the cylinder liner, six test groups were performed, with stopping conditions set at 30 minutes, 60 minutes, 120 minutes, 180 minutes, Cof = 0.25, and Cof = 0.3. After each test, the samples were cleaned again with petroleum ether and anhydrous ethanol for 5 minutes each to remove any residual surface oil. Each test group was repeated at least three times to ensure the reliability and repeatability of the results.

The wear scar morphology of the cylinder liner and piston ring was measured using a white light interferometer to assess the degree of wear. The microstructure and wear scar morphology of the samples were observed using an optical microscope (OM) and scanning electron microscope (SEM). The changes and distribution characteristics of elements on the worn surfaces were examined using an energy dispersive spectrometer (EDS). A focused ion beam (FIB) technique was employed to cut a thin slice from a specific area of the wear scar to prepare a TEM sample. The morphology and characteristics of the tribo-layer in the wear scar were observed using transmission electron microscopy (TEM) and high-resolution transmission electron microscopy (HRTEM) to analyze the wear transition mechanism. Fig. 3 provides a schematic diagram of the test and analysis process.

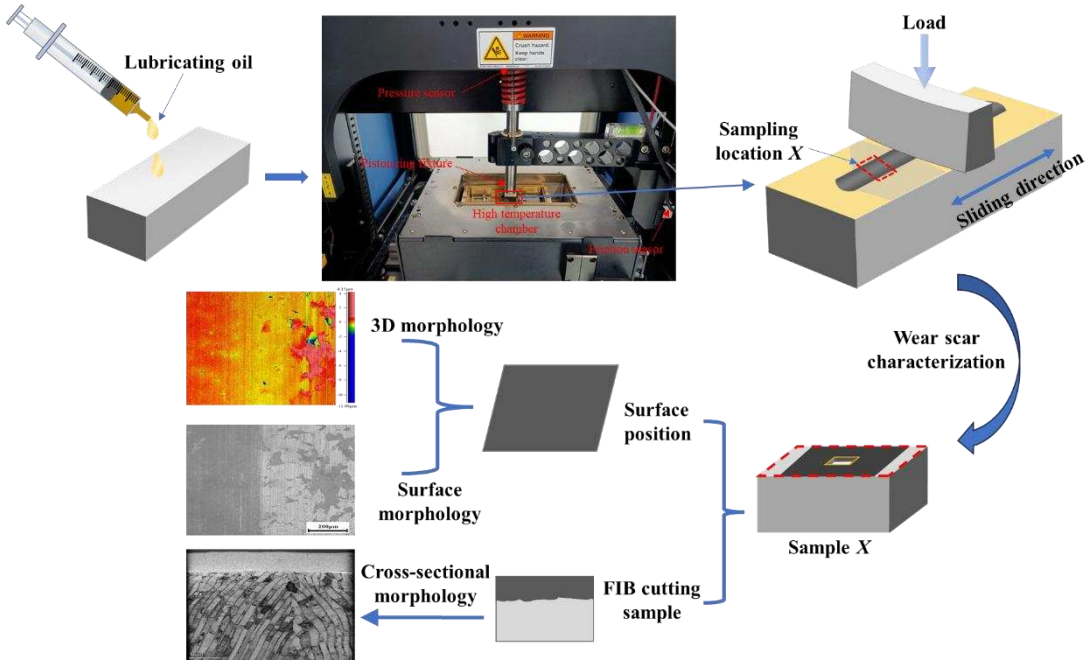

Fig. 3. Schematic diagram of the test and analysis process.

3. Results

3.1 Variation of friction coefficient

Fig. 4 shows the friction coefficient and the average values from three repeated tests at each stage, corresponding to loads of 50N, 100N, 200N, and 300N, with Cof values of 0.25 and 0.3, respectively. Due to directional changes during the reciprocating sliding wear process, the friction coefficient displays a jagged pattern, as shown by the light-colored lines in Fig. 4 (a). To more clearly illustrate the friction coefficient's variation trend during the wear tests, a low-pass filter with a cutoff frequency of 0.1 was applied to the original data. The filtered result is represented by the dark-colored curve in Fig. 4 (a). The red curve in Fig. 4 (a) illustrates the overall trend of the friction coefficient throughout the test. It shows that the friction coefficient increases rapidly within a short period at the beginning of the test when the applied load is 50N. As the load increases to 100N, the friction coefficient gradually decreases, possibly due to the formation of a self-lubricating layer on the surface [36, 37]. As the load continues to increase to 200N, the friction coefficient rises slowly and then stabilizes. After a prolonged stable phase, with the load reaching 550N, the friction coefficient increases rapidly until it reaches Cof = 0.3, at which point the test is stopped. The results from the other test groups in Fig. 4 (a) show a trend consistent with the various stages

observed in the complete test. Fig. 4 (b) illustrates the variation in the average friction coefficient from repeated tests as the load increases in 50N increments. It can be observed that when the load is between 50N and 150N, the friction coefficient decreases as the load increases. Between 150N and 300N, the friction coefficient gradually rises with the load and remains stable between 300N and 450N. Once the load exceeds 450N, the friction coefficient continues to increase until the instantaneous value reaches 0.3, at which point the test is stopped with the load at 550N. This pattern is consistent with the results shown in Fig. 4 (a). The results in Fig. 4 (b) represent the average friction coefficient, which is notably lower than the instantaneous values. This trend aligns with the general friction coefficient patterns observed under dry friction conditions, although under starved lubrication, the friction coefficient is lower, and each phase lasts longer compared to dry friction conditions [32].

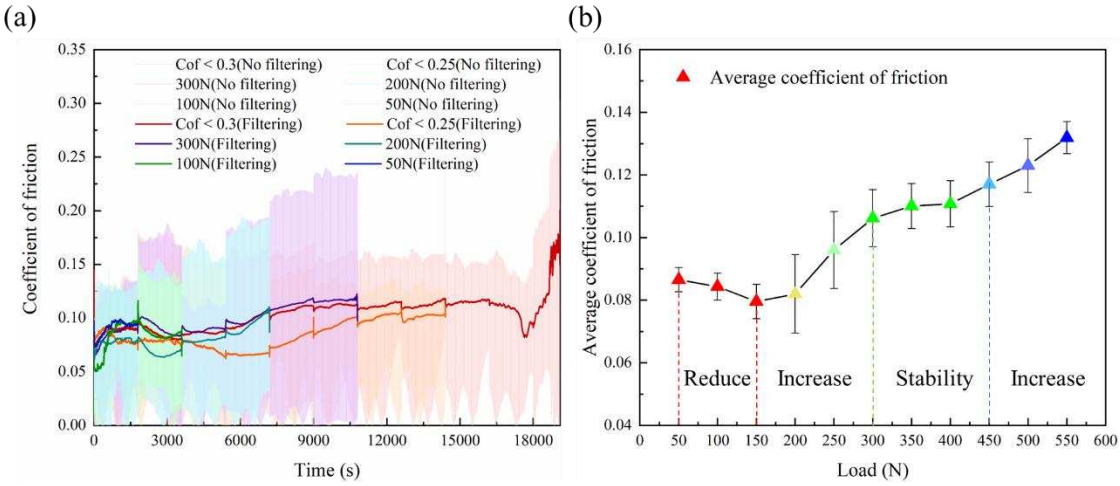

Fig. 4. The variation of the friction coefficient: (a) the changes in the friction coefficient at loads of 50N, 100N, 200N, and 300N, as well as at Cof = 0.25 and Cof = 0.3, (b) the variation in the average friction coefficient from repeated tests as the load increases by 50N increments.

3.2 Variation of wear loss

Fig. 5 illustrates the wear scar morphology characteristics of the cylinder liner and piston ring at different wear stages. A white light interferometer was used to measure the three-dimensional and one-dimensional morphological changes at the wear scar locations on the cylinder liner and piston ring to assess the variation in wear loss at different stages. Based on the changes in the friction coefficient, several key points during the test were identified: first, within the initial 30 minutes (load of 50N), where

the friction coefficient rapidly increased; second, at 60 minutes (load of 100N), when the friction coefficient decreased; third, just before scuffing occurred (Cof = 0.25); and finally, when scuffing occurred (Cof = 0.3). The wear amount at these key points was measured.

From the changes in the wear scar depth on the cylinder liner (Fig. 5 (a3)), it can be observed that the wear loss at 50N and 100N was minimal, with only changes in the surface roughness of the wear scar, and no significant changes in wear depth were detected. However, when the friction coefficient increased to 0.25, both the wear scar depth and width increased significantly, indicating more severe wear on the cylinder liner. When the friction coefficient further increased to 0.3, the wear scar depth increased further, and the wear scar shape became irregular. The cross-sectional morphology of the wear scar on the piston ring is shown in Fig. 5 (b3), and its wear pattern is largely consistent with that of the cylinder liner. When the load was 50N and 100N, the wear was relatively light. As the load increased, the wear depth also increased, and when the friction coefficient reached 0.3, the surface morphology of the wear scar became irregular, indicating a more pronounced scuffing phenomenon between the piston ring and the cylinder liner.

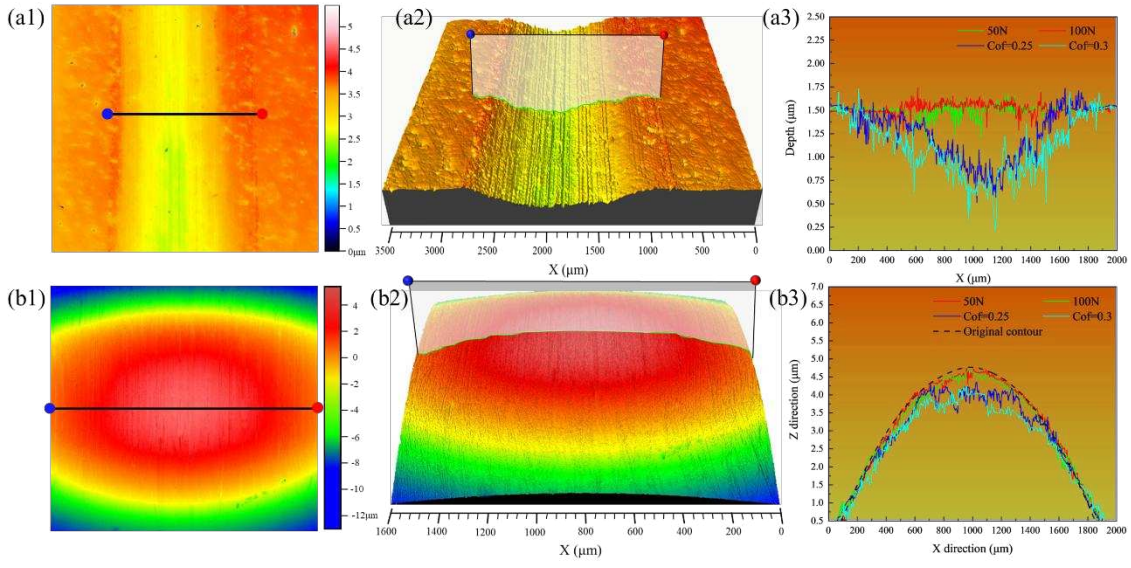

Fig. 5. Characteristics of wear scar morphology of cylinder liner and piston ring: (a) cylinder liner, (b) piston ring, (1) two-dimensional diagram of wear scar morphology, (2) three-dimensional diagram of wear scar morphology (3) cross-section profile of wear scar under different parameters.

3.3 Surface characteristics of wear scars

To analyze the variation patterns of wear states at different stages, an optical microscope was used to observe the morphology of wear scars at key points. When the load was 50N, noticeable wear marks appeared at the wear scar locations, with a clear color difference between the worn and unworn areas. The wear scar areas were darker, indicating that a tribo-layer may have formed on the surface of the wear scar. However, large volumes of graphite and the edges of the graphite were not covered by this tribo-layer, as evidenced by the corresponding three-dimensional morphology, where a significant height difference was observed between the graphite edges and the areas covered by the tribo-layer. When the load increased to 100N (Fig. 6 (b)), the tribo-layer on the surface became more uniform and compact. The three-dimensional morphology also showed that the surface roughness parameter Sa=0.062, which was lower than the roughness value at 50N. This indicates that the surface became smoother as the load increased to 100N, which could be one of the reasons for the reduction in the friction coefficient. Additionally, it also shows that apart from a few large graphite areas that were not covered by the tribo-layer, some eutectic phosphorus regions were also uncovered, suggesting that it is difficult for the tribo-layer to form on the eutectic phosphorus surface. When the load increased further and the friction coefficient reached 0.25 (Fig. 6 (c)), small flaky graphite covered by the tribo-layer could be observed in the middle of the wear scar, indicating that wear on the tribo-layer had occurred, leading to a reduction in its thickness. Due to the higher pressure in the middle of the wear scar, the wear there was greater than at the edges, forming a sharp contrast between the middle and edge regions. Additionally, the three-dimensional morphology revealed that the wear in the middle was more severe, causing an increase in surface roughness. When the load further increased and the friction coefficient reached 0.3 (Fig. 6 (d)), severe wear and delamination of the tribo-layer occurred in some parts of the wear scar, leading to a further increase in surface roughness. This is also the reason for the rapid rise in the friction coefficient.

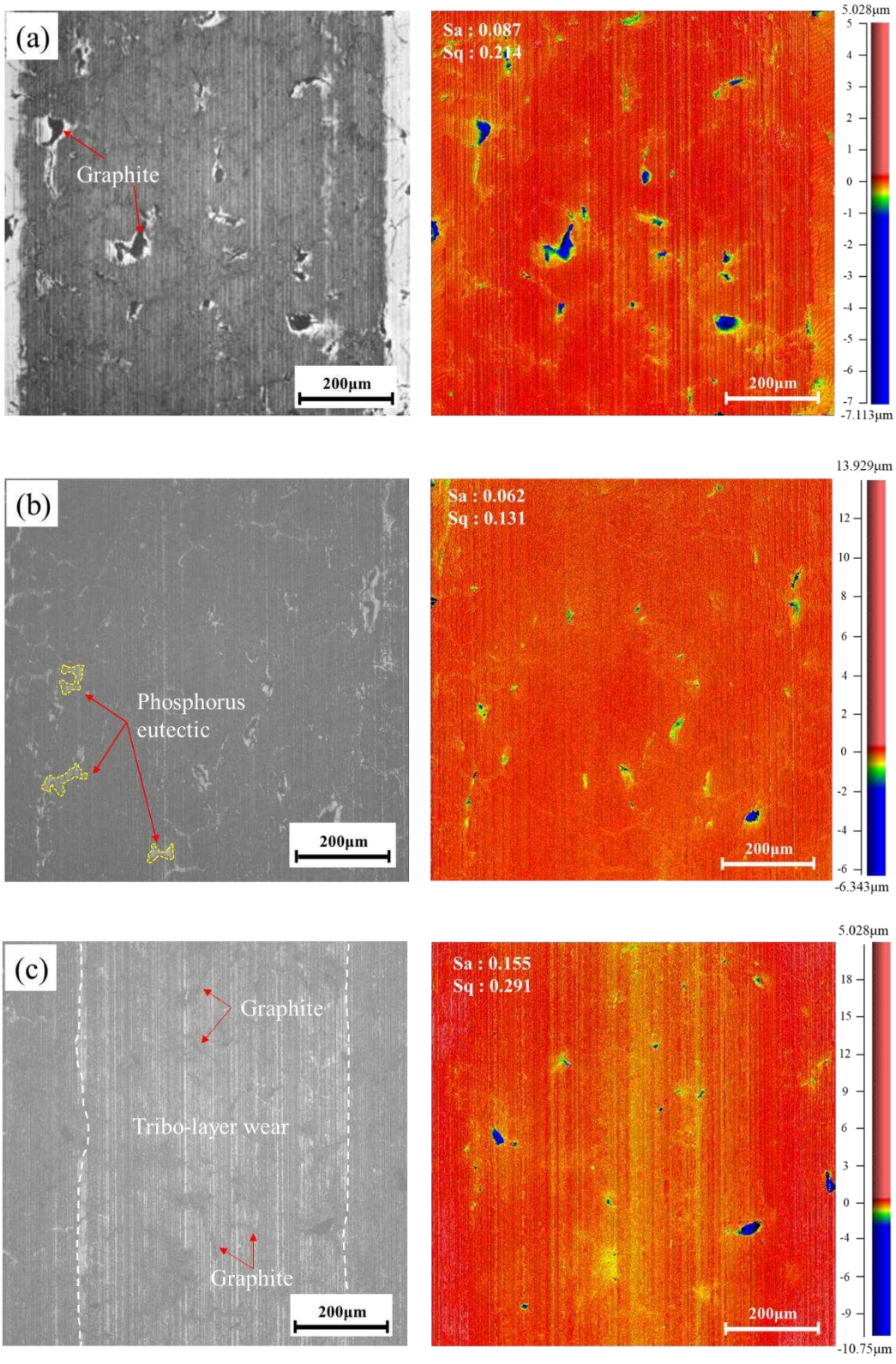
(a)
Graphite
200μm
Sa : 0.087
Sq : 0.214
200μm
5.028μm
5
4
3
2
1
0
-1
-2
-3
-4
-5
-6
-7
-7.113μm
(b)
Phosphorus
eutectic
200μm
Sa : 0.062
Sq : 0.131
200μm
13.929μm
12
10
8
6
4
2
0
-2
-4
-6
-6.343μm
(c)
Graphite
Tribo-layer wear
Graphite
200μm
Sa : 0.155
Sq : 0.291
200μm
5.028μm
18
15
12
9
6
3
0
-4
-6
-9
-10.75μm

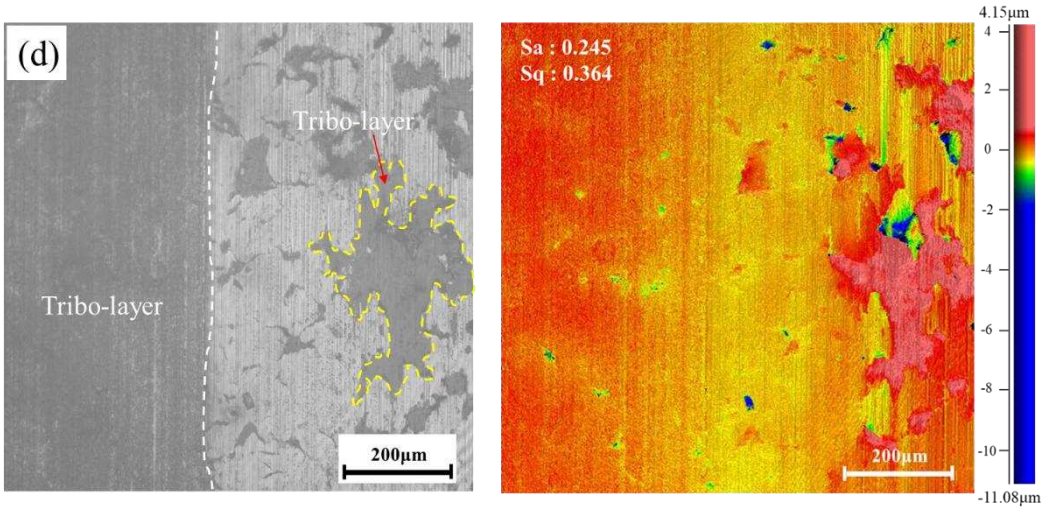

Fig. 6. The surface and three-dimensional morphology characteristics of cylinder liner wear scars under the optical microscope: (a) 50N, (b) 100N, (c) Cof = 0.25, (d) Cof = 0.3.

Fig. 7 shows the wear scar morphology and elemental distribution observed under a scanning electron microscope (SEM) at different wear stages, providing a more accurate assessment of the transition in wear mechanisms. Fig. 7 (a) illustrates the wear scar morphology at a load of 50N. It can be seen that a tribo-layer has begun to form on the wear scar surface, and some graphite has already been covered by this tribo-layer. From the localized magnified image (Fig. 7 (a2)), it is evident that the eutectic phosphorus surface is not covered by the tribo-layer, while some areas of graphite are. Based on the EDS spectrum, it can be inferred that the tribo-layer has a high oxygen content, indicating that the formation of the tribo-layer may be related to surface oxidation. Additionally, the oxygen distribution map shows lower oxygen content on the eutectic phosphorus surface, further proving that the tribo-layer does not form on the eutectic phosphorus surface. When the load increased to 100N (Fig. 7 (b)), as seen in Fig. 6, the tribo-layer became more compact. However, areas near larger volumes of graphite and the eutectic phosphorus still exposed the substrate, indicating that these regions were not fully covered by the tribo-layer. In addition, larger graphite particles had already detached, creating localized defects. As the load continued to increase and the friction coefficient rose to 0.25, clear plowing marks appeared on the tribo-layer surface, along with localized adhesive wear, indicating that significant wear of the tribo-layer had begun. Furthermore, the localized magnified image (Fig. 7 (c2)) also showed

that the eutectic phosphorus was not covered by the tribo-layer, confirming that the eutectic phosphorus surface remains uncovered throughout the tribo-layer formation process. When the load further increased and the friction coefficient rose to 0.3 (Fig. 7 (d)), severe scuffing occurred on the cylinder liner surface, and large areas of the tribo-layer had worn away. The localized magnified image (Fig. 7 (d2)) reveals micro-cracks at the edge of the tribo-layer, and small wear debris was observed on the exposed substrate where the tribo-layer had detached. This indicates that the detachment of the tribo-layer resulted in direct contact between the piston ring and the cylinder liner substrate, leading to scuffing.

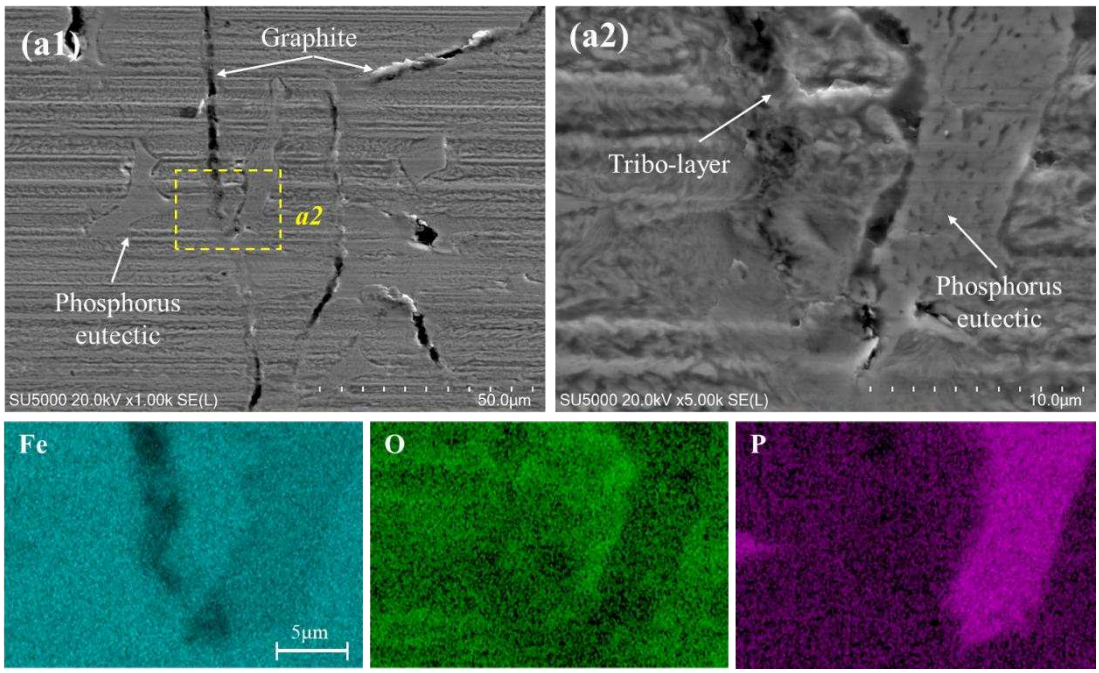

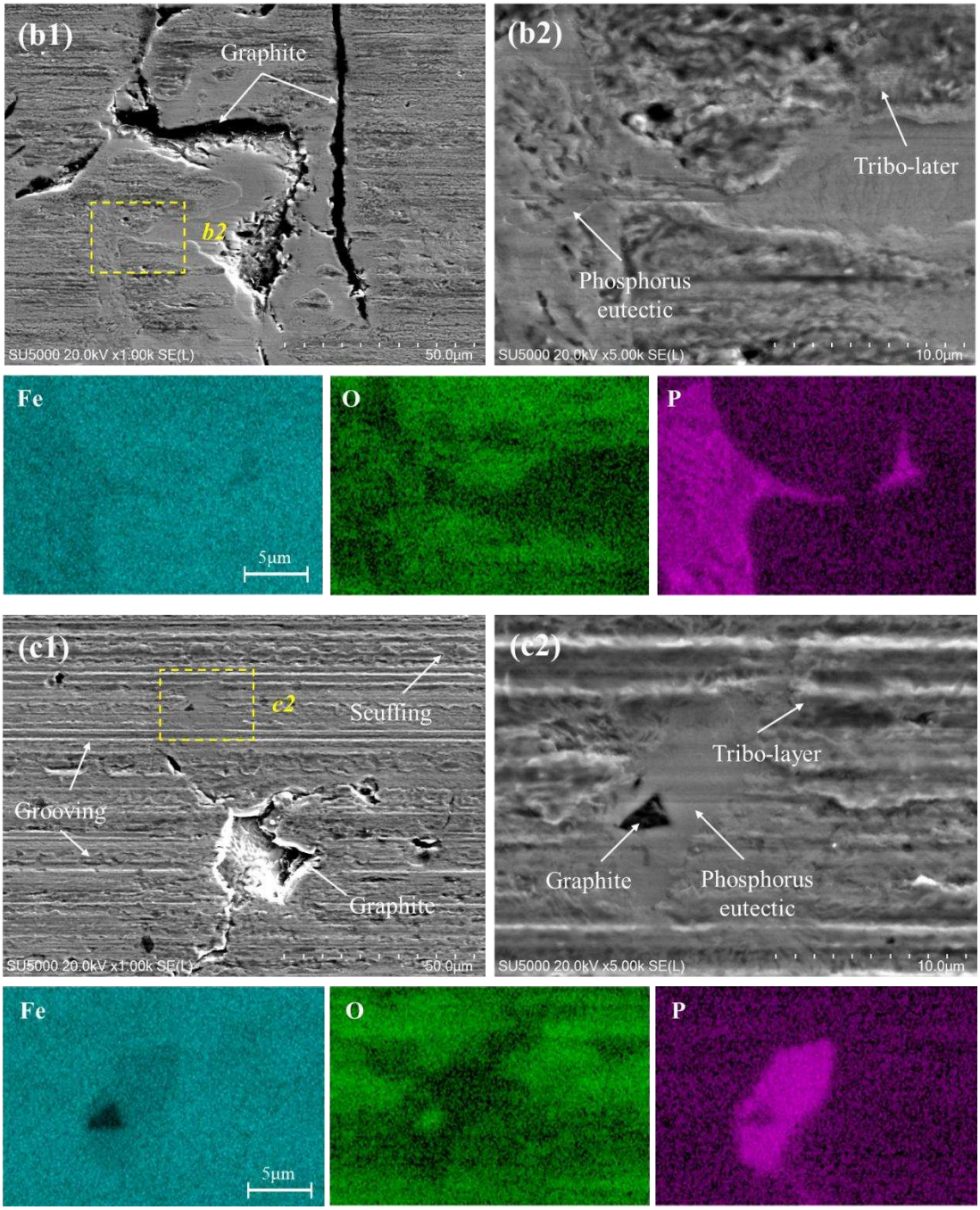
(b1)
Graphite
b2
SU5000 20.0kV x1.00k SE(L)
50.0μm
(b2)
Tribo-later
Phosphorus
eutectic
SU5000 20.0kV x5.00k SE(L)
10.0μm
Fe
5μm
O
P
(c1)
c2
Scuffing
Grooving
Graphite
SU5000 20.0kV x1.00k SE(L)
50.0μm
(c2)
Tribo-layer
Graphite
Phosphorus
eutectic
SU5000 20.0kV x5.00k SE(L)
10.0μm
Fe
5μm
O
P

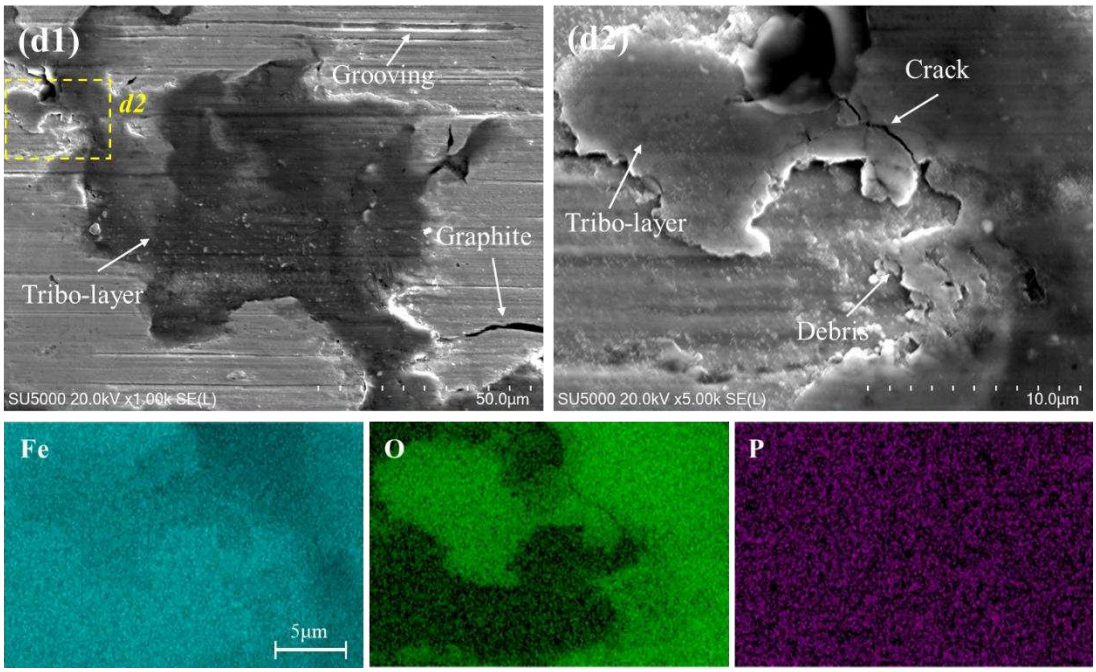

Fig. 7. Wear scar morphology and EDS spectrum at different wear stages: (a) 50N, (b) 100N, (c) Cof = 0.25, (d) Cof = 0.3, (1) macro morphology of wear scar, (2) corresponding to local position amplification in (1).

Fig. 8 shows the wear scar morphology and EDS spectra of the piston ring under different wear conditions. When the load is relatively low, the piston ring experiences minimal wear, and the initial surface morphology of the coating remains visible. As the load increases to 100N, the initial machining marks on the coating surface become shallower, and the wear scar surface appears smooth, with no evidence of material transfer from the cylinder liner. This indicates that while wear has occurred, no scuffing has taken place at this stage. When the load increases further and the friction coefficient reaches 0.25, there are clear signs of scuffing on the piston ring surface. According to the EDS spectrum at point P1 (Fig. 8 (P1)), the surface is rich in oxygen (O) and iron (Fe) elements, indicating that the tribo-layer from the cylinder liner has transferred to the piston ring surface, signifying adhesive wear. As the load continues to increase and the friction coefficient reaches 0.3, the scuffing on the piston ring surface becomes even more pronounced, with larger amounts of wear debris transferred to the piston ring surface (Fig. 8 (d)). The EDS spectrum at point P2 shows that the transferred wear debris also originates from the tribo-layer of the cylinder liner.

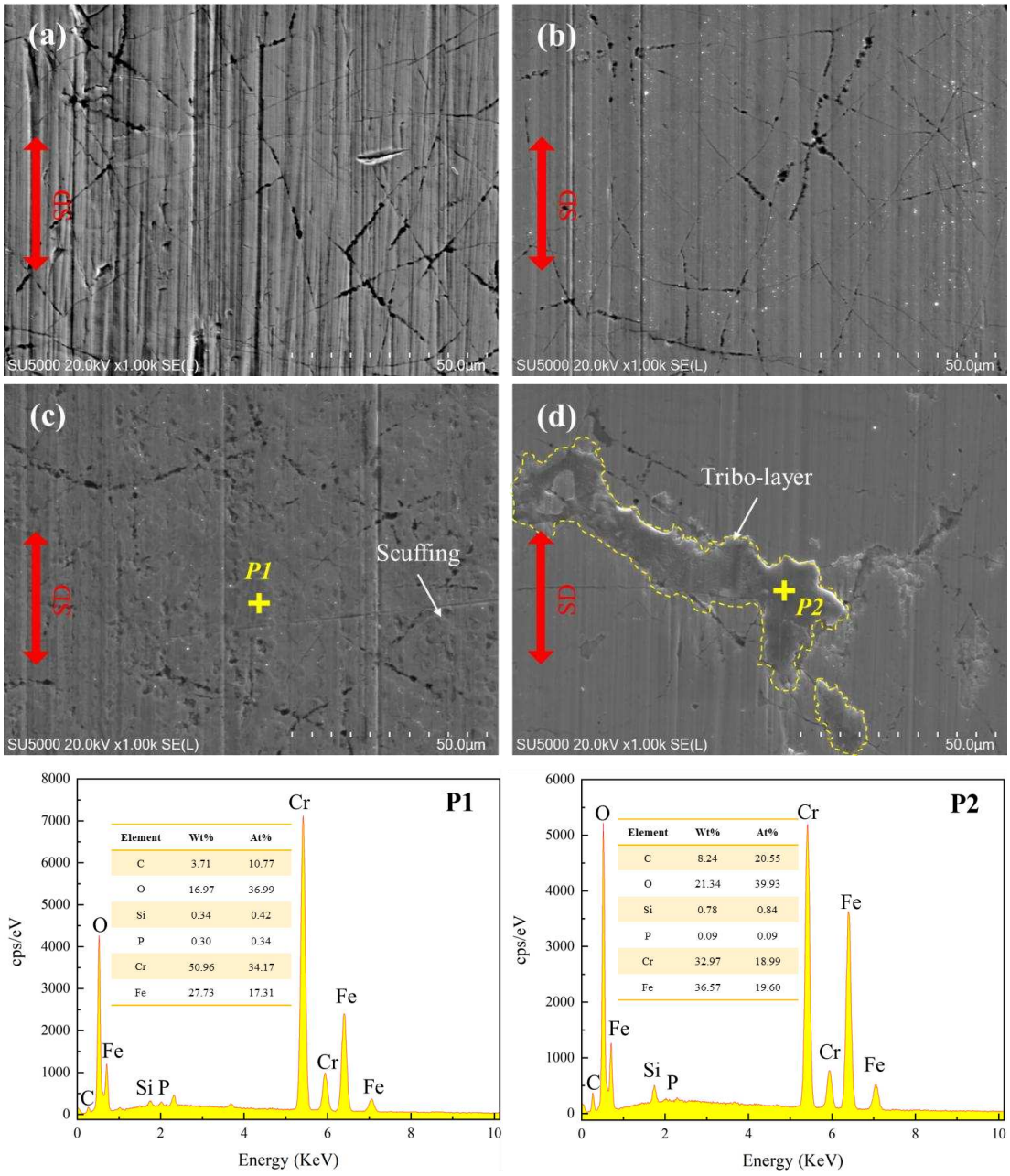

Fig. 8. Surface morphology and EDS energy spectrum of piston ring wear scar.

3.3 Cross-section characteristics of wear scar

Based on the above analysis, it is evident that the wear characteristics of the cylinder liner depend on the transformation of the frictional interface features. To investigate the mechanism of scuffing and the structure of the tribo-layer, focused ion beam (FIB) technology was used to precisely cut samples from the tribo-layer on the wear scar surface of the cylinder liner for cross-sectional analysis. During the complete test, the reduction in the friction coefficient at a load of 100N and the occurrence of scuffing when the friction coefficient reached 0.3 were noteworthy, so the cross-sections of the

tribo-layers at these two moments were analyzed. Fig. 9 shows the surface interface images of the tribo-layer on the wear scar when the load was 100N. From Fig. 9 (a), it can be seen that the wear scar surface is covered by a tribo-layer, which acts as the primary contact carrier. The reduction in the friction coefficient is primarily due to the formation of this tribo-layer. Fig. 9 (b) shows the sampling process. Fig. 9 (c) illustrates the cross-sectional morphology of the FIB-cut sample, revealing that the wear scar surface is covered by a tribo-layer approximately 187nm thick. This layer has an uneven thickness that varies with the surface topography of the substrate, and its coverage reduces the surface roughness of the substrate, which is consistent with the results in Fig. 6 (b). From the localized magnified image (Fig. 9 (d)), it can be seen that the tribo-layer consists of densely packed nanoparticles. Elemental analysis shows that this tribo-layer is rich in iron (Fe) and oxygen (O), with small amounts of phosphorus (P), and zinc (Zn), which are likely related to anti-wear additives in the lubricating oil [38]. Further magnification of the tribo-layer (Fig. 9 (f)) reveals that the nanoparticles have diameters of approximately 5-20nm, with key elements including Fe, O, chromium (Cr), and carbon (C). Fast Fourier transform (FFT) analysis of individual nanoparticles under high-resolution transmission electron microscopy (HRTEM) (Fig. 9 (h)) shows that the tribo-layer is primarily composed of Fe_2O_3 nanocrystals.

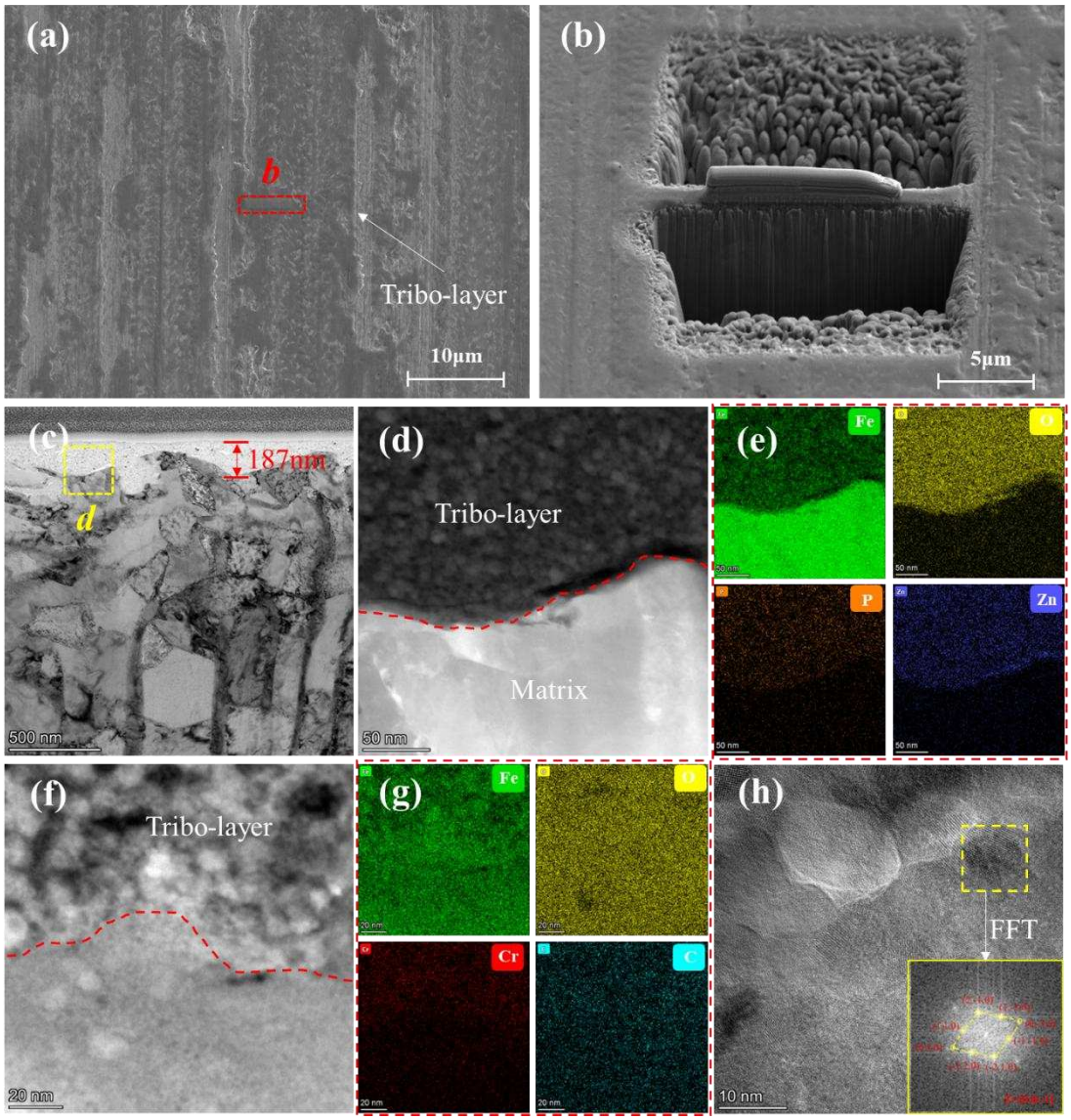

Fig. 9. TEM sample preparation and characterization of tribo-layer cross-section when the load is 100N：(a) Wear scar surface tribo-layer and FIB sampling position，(b) FIB sample preparation process， local amplification of position *b* in (a)，(c) Bright-field TEM images of tribo-layer cross-section，(d) The HAADF image of the local position *d* in (c)，(e) The element distribution of (d)，(f) Local magnification of the tribo-layer in (d)，(g) The element distribution of (f)，(h) HRTEM image of (f) and fast-Fourier transform (FFT) image of selected area position.

Fig. 10 shows the cross-sectional transmission electron microscope (TEM) images of the unworn tribo-layer on the wear scar surface of the cylinder liner when severe scuffing occurred (Cof = 0.3). In Fig. 10 (a), it is evident that a distinct tribo-layer exists

at the wear scar location, and part of this layer has already experienced wear. Fig. 10 (b) shows the position where the sample was cut. Fig. 10 (c) presents the cross-sectional morphology of the wear scar, revealing a lamellar pearlite structure in the substrate. The tribo-layer at this stage is about 836nm thick, significantly thicker than the layer observed at the load of 100N, indicating that the thickness of the tribo-layer increases as the wear process progresses. Additionally, microcracks are evident at the interface between the tribo-layer and the substrate, which may be one of the primary reasons for the detachment of the tribo-layer from the substrate, leading to scuffing. Elemental analysis of the tribo-layer shows that it is primarily enriched with iron (Fe) and oxygen (O) (Fig. 10 (e)), with small amounts of phosphorus (P) and zinc (Zn) detected. Notably, zinc enrichment is observed in the crack locations, suggesting that the formation of these cracks may be related to the presence of a tribofilm. To further analyze the structure of the tribo-layer, the local region of the layer was magnified to observe its composition at a higher magnification. As shown in Fig. 10 (f), the tribo-layer is still composed of densely packed nanocrystals, with the crystal size and elemental composition similar to the tribo-layer observed under the 100N load. Fast Fourier transform (FFT) analysis of the nanocrystals in the high-resolution TEM images confirms that the tribo-layer is still primarily composed of Fe_2O_3 nanocrystals.

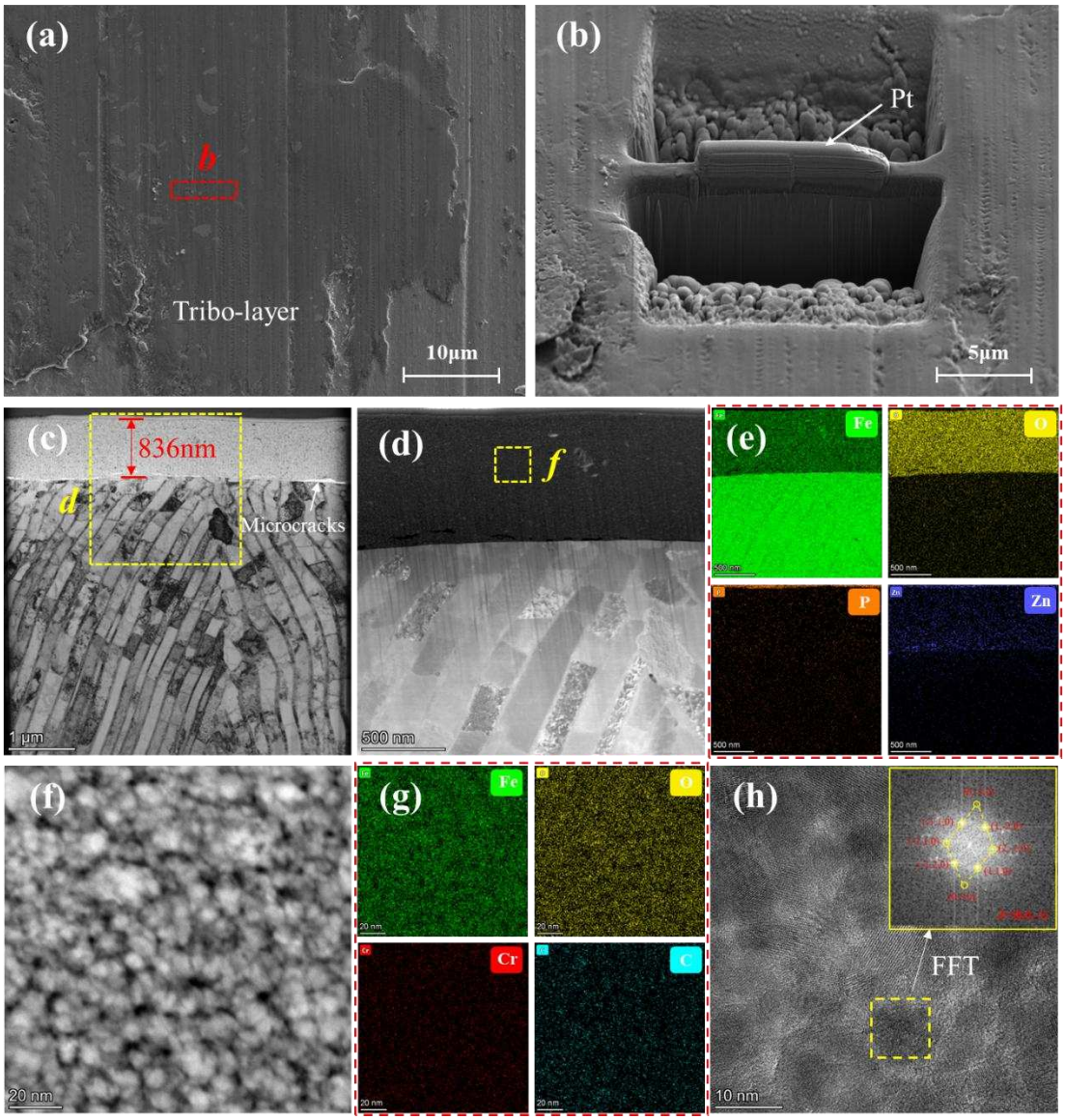

Fig. 10. TEM sample preparation and characterization of tribo-layer cross-section when Cof= 0.3：(a) Wear scar surface tribo-layer and FIB sampling position，(b) FIB sample preparation process， local amplification of position b in (a)，(c) Bright-field TEM images of tribo-layer cross-section，(d) The HAADF image of the local position d in (c)，(e) The element distribution of (d)，(f) local magnification of the tribo-layer in (d)，(g) The element distribution of (f)，(h) HRTEM image of (f) and fast-Fourier transform (FFT) image of selected area position.

4. Discussion

Based on the above analysis, it is evident that the wear state of the cylinder liner and piston ring under starved lubrication conditions changes with the load, and these

wear state transitions are closely related to the changes in the characteristics of the contact interface. According to the variation in the friction coefficient, at the beginning of the test, the surface roughness of the cylinder liner is low due to its grinding and polishing treatment, and the graphite on the surface easily wears off. The detached graphite affects the contact surface in two ways: first, the graphite particles enter the friction system, and due to graphite's inherent lubricating properties, they reduce the friction coefficient between the cylinder liner and the piston ring [39, 40]； Second, the pits left by the detached graphite increase the surface roughness of the cylinder liner, enhancing contact stability and causing the friction coefficient to rise. As shown in the results of Fig. 4 (a), the friction coefficient rises rapidly after a brief period of stabilization when the load is 50N. This indicates that, in the early stages of friction, the surface characteristics and the lubricating effects of graphite and oil result in a lower friction coefficient. Subsequently, a tribo-layer begins to form, with small volumes of graphite being covered by the tribo-layer (Fig. 7 (a2)), preventing further release of graphite. However, the tribo-layer is not fully formed at this stage, especially around eutectic phosphorus and large volumes of graphite, leading to an increase in surface roughness (Fig. 6 (a)) and, consequently, a rise in the friction coefficient.

When the load increases to 100N, the friction coefficient decreases significantly. This phenomenon is mainly due to the increase in the thickness of the tribo-layer and its self-lubricating effect. As the load increases, the coverage area and thickness of the tribo-layer increase, making the tribo-layer the primary contact surface with the piston ring. Although some localized areas remain uncovered (Fig. 7 (b2)), the density and thickness of the tribo-layer on the surface have increased noticeably compared to the 50N load (Fig. 6 (b)). The self-lubricating properties of the tribo-layer have been reported in the literature. Yin et al. [36] found that for materials with martensitic or pearlitic structures, a thin self-lubricating layer composed of nanoparticles (6-20nm) forms under specific strain levels, transitioning the material from severe to mild wear. This aligns with the results observed in this study (Fig. 9). As the load continues to increase, the thickness of the tribo-layer exhibits a trend of first increasing and then decreasing, depending on the competition between the growth rate of the tribo-layer and the wear rate [41]. At lower loads, no material transfer from the cylinder liner to

the piston ring is observed, and the tribo-layer becomes denser, enhancing the self-lubricating effect. However, as the load increases, noticeable material transfer from the cylinder liner to the piston ring occurs (Fig. 8 (c)), indicating the wear of the tribo-layer. Regarding the wear mechanism of the tribo-layer, Saeidi et al. [31] suggested that the reduction of the tribo-layer to α-Fe triggers adhesive wear of the layer. The adhesive effect between the tribo-layer and the piston ring weakens the self-lubricating properties, leading to an increase in the friction coefficient.

As the load increases further, the rising friction coefficient causes increased shear stress, leading to large-scale detachment of the tribo-layer. The reasons for the detachment of the tribo-layer can be summarized as follows: first, areas around eutectic phosphorus and large graphite volumes are difficult to cover with the tribo-layer (Fig. 6 and Fig. 7), making these locations stress concentration points where microcracks form, resulting in the detachment of the tribo-layer. Second, the graphite covered by the tribo-layer can also induce stress concentrations, leading to microcracks between the tribo-layer and the substrate. The propagation of these cracks causes large portions of the tribo-layer to adhere to the piston ring, resulting in adhesive wear, consistent with previously reported findings [9, 31]. Lastly, the formation of these cracks may be related to the tribofilm present during the early stages of wear. When tribofilm form or accumulates in localized areas and are subsequently covered by the tribo-layer, these films become crack initiation sites. When shear stress increases, cracks can form and propagate from these locations. This conclusion can be inferred from the results of Fig. 10. It should be noted that, in this study, no clear tribofilm was observed on the wear scar surface, likely due to the starved lubrication conditions. The low amount of lubricating oil may have been insufficient to form large-scale tribofilm on the wear surface. Additionally, the wear rate of tribofilm may have exceeded their formation rate, contributing to this phenomenon. Fig. 11 provides a schematic diagram of adhesive wear.

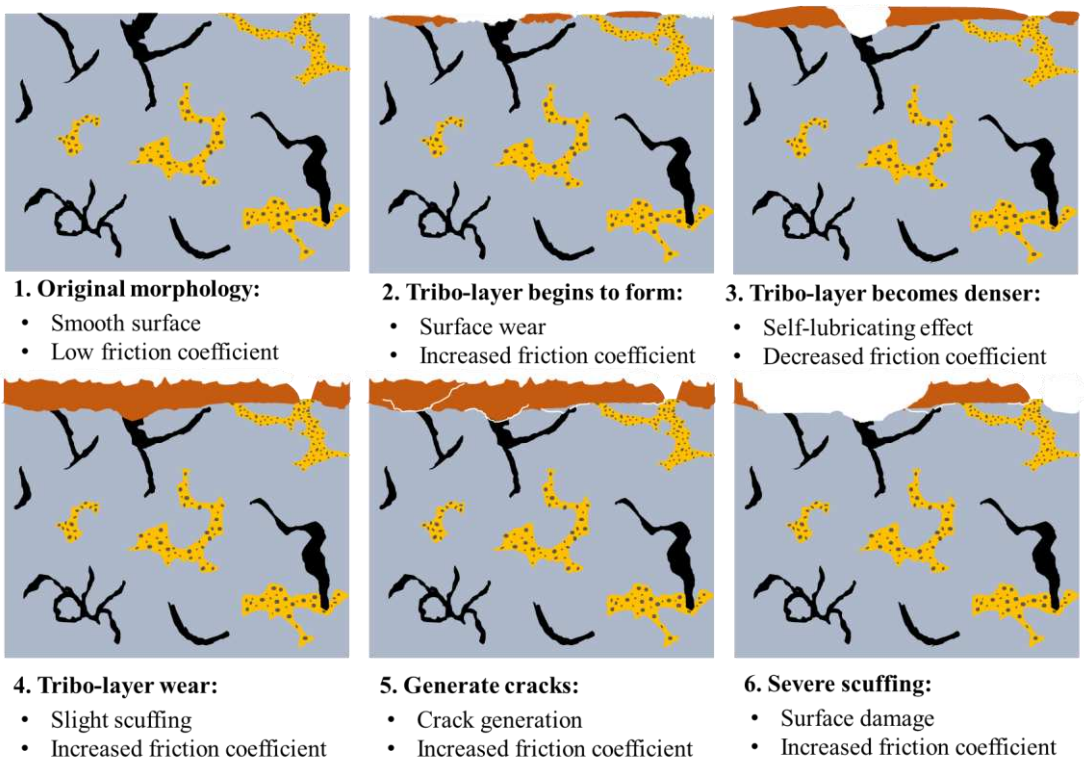

Fig. 11 Schematic diagram of the scuffing process of the cylinder liner.

5. Conclusion

Sliding wear tests were conducted under starved lubrication conditions using piston rings and cylinder liners. By analyzing the changes in friction coefficient, wear loss, and surface morphology characteristics of the cylinder liner and piston ring interfaces at different stages, the wear state transitions of the cylinder liner and the mechanisms leading to severe scuffing were investigated. The following conclusions can be drawn:

1. Under starved lubrication conditions, a tribo-layer with self-lubricating properties forms on the surface of the cylinder liner. This tribo-layer can reduce the friction coefficient under low load conditions. However, the detachment of the tribo-layer is also a key factor contributing to severe scuffing.
2. The microstructure of the cylinder liner material also affects the formation of the friction layer. Typically, the friction layer adheres to the surface of pearlite, while larger volumes of graphite and phosphorus eutectic surfaces are difficult to cover.
3. The tribo-layer is primarily composed of 5-20nm iron oxide nanocrystals. Its formation is mainly due to wear debris being repeatedly compacted under the

conditions of the friction system, resulting in a dense oxide film.

4. When the tribo-layer completely detaches, the friction coefficient increases rapidly. The graphite and eutectic phosphorus in the cylinder liner are the primary sources of crack formation. Additionally, the formation or accumulation of an initial tribofilm on the surface also contributes to the generation of cracks.

Reference:

[1] B.-K.Z. Chui, Computational analysis of piston ring wear and oil consumption for an internal combustion engine, 2001.

[2] R. Rahmani, H. Rahnejat, B. Fitzsimons, D. Dowson, The effect of cylinder liner operating temperature on frictional loss and engine emissions in piston ring conjunction, Applied Energy, 191 (2017) 568-581. https://doi.org/10.1016/j.apenergy.2017.01.098

[3] S. Dahdah, N. Biboulet, A. Lubrecht, P. Charles, Scuffing initiation caused by local starvation in a piston ring cylinder liner contact, Tribology International, 172 (2022) 107616. https://doi.org/10.1016/j.triboint.2022.107616

[4] Z.Q. Wang, J.J. Xu, Tribology in piston ring cylinder liner system of diesel engine, Science Press, Beijing, 2021.

[5] P. Papadopoulos, M. Priest, W.M. Rainforth, Investigation of fundamental wear mechanisms at the piston ring and cylinder wall interface in internal combustion engines, Proceedings of the institution of mechanical engineers part J-Journal of engineering tribology 221 (2007) 459-459.

[6] P. Olander, S.S. Eskildsen, J.W. Fogh, P. Hollman, S. Jacobson, Testing scuffing resistance of materials for marine 2-stroke engines – Difficulties with lab scale testing of a complex phenomenon, Wear, 340-341 (2015) 9-18. https://doi.org/10.1016/j.wear.2015.06.015

[7] J. Gussmagg, M. Pusterhofer, F. Summer, F. Grün, Experimental visualization of the wear and scuffing evolution of a flake graphite cast iron cylinder liner, Wear, 526-527 (2023) 204948. https://doi.org/10.1016/j.wear.2023.204948

[8] J. Nadel, T.S. Eyre, Cylinder liner wear in low speed diesel engines, Tribology International, 11 (1978) 267-271. https://doi.org/10.1016/0301-679X(78)90056-7

[9] B. Zhang, X. Ma, L. Liu, H. Yu, A. Morina, X. Lu, Study on the sliding wear map of cylinder liner − piston ring based on various operating parameters, Tribology International, 186 (2023) 108632. https://doi.org/10.1016/j.triboint.2023.108632

[10] J. Nadel, T.S. Eyre, Cylinder liner wear in low speed diesel engines, Tribology

International, 11 (1978) 267-271. https://doi.org/10.1016/0301-679X(78)90056-7

[11] M.F. Jensen, J. Bøttiger, H.H. Reitz, M.E. Benzon, Simulation of wear characteristics of engine cylinders, Wear 253 (2002) 1044-1056. https://doi.org/10.1016/S0043-1648(02)00251-X

[12] T.J. Kamps, J.C. Walker, R.J. Wood, P.M. Lee, A.G. Plint, Reproducing automotive engine scuffing using a lubricated reciprocating contact, Wear, 332 (2015) 1193-1199. https://doi.org/10.1016/j.wear.2014.12.045

[13] J.C. Walker, H.G. Jones, T.J. Kamps, Dynamic pressure scuffing initiation of a grade 250 flake graphite cast iron, Wear, 523 (2023) 204864. https://doi.org/10.1016/j.wear.2023.204864

[14] B. Li, C.H. Wong, Q. Chen, Kinetics of lubricant desorption and decomposition under heat treatment: A molecular dynamics study, Soft Matter, 9 (2013) 700-708. https://doi.org/10.1039/c2sm26973b

[15] K. Yagi, H. Tango, T. Izumi, M. Tohyama, K. Saito, J. Sugimura, In-situ observation of influence of metal types on wear process in dry conditions, Wear, 488-489 (2022) 204162. https://doi.org/10.1016/j.wear.2021.204162

[16] T. Wopelka, U. Cihak-Bayr, C. Lenauer, F. Ditroi, S. Takács, J. Sequard-Base, M. Jech, Wear of different material pairings for the cylinder liner – piston ring contact, Industrial Lubrication and Tribology, 70 (2018) 687-699. https://doi.org/10.1108/ILT-07-2017-0218

[17] J.M. Han, Q. Zou, G.C. Barber, T. Nasir, D.O. Northwood, X.C. Sun, P. Seaton, Study of the effects of austempering temperature and time on scuffing behavior of austempered Ni – Mo – Cu ductile iron, Wear, 290-291 (2012) 99-105. https://doi.org/10.1016/j.wear.2012.05.003

[18] Y. Wang, Z. Sun, R. Huang, Z. Zhao, W. Zhang, Tribological Properties of Several Surface-Modified Piston Rings Under Extreme Conditions, Journal of Tribology, 146 (2023). https://doi.org/10.1115/1.4063187

[19] S. Wan, D. Li, G.a. Zhang, A.K. Tieu, B. Zhang, Comparison of the scuffing behaviour and wear resistance of candidate engineered coatings for automotive piston

rings, Tribology International, 106 (2017) 10-22. https://doi.org/10.1016/j.triboint.2016.10.026

[20] Z. Liu, F.X. Liang, L.M. Zhai, X.H. Meng, A comprehensive experimental study on tribological performance of piston ring-cylinder liner pair, Proceedings of the Institution of Mechanical Engineers Part J-Journal of Engineering Tribology, 236 (2022) 184-204. https://doi.org/10.1177/13506501211004758

[21] Y. Matsuzaki, K. Yagi, J. Sugimura, Investigation of influence of lubricant additives on scuffing performance using in-situ observation method, Proceedings Of Asia International Conference On Tribology 2018 (ASIATRIB 2018), pp. 219-221.

[22] J.H. Horng, T.N. Ta, Y.S. Wu, Analysis of surface damage characteristics and scuffing prediction in the presence of ZDDP additive and running-in process, Jurnal Tribologi, 41 (2024) 177-191.

[23] B. Podgornik, Adhesive Wear Failures, Journal of failure analysis and prevention 22 (2022) 113-138. https://doi.org/10.1007/s11668-021-01322-4

[24] O.O. Ajayi, C. Lorenzo-Martin, R.A. Erck, G.R. Fenske, Scuffing mechanism of near-surface material during lubricated severe sliding contact, Wear, 271 (2011) 1750-1753. https://doi.org/10.1016/j.wear.2010.12.086

[25] H.A. Blok, Theoretical Study of Temperature Rise at Surface of Actual Contact Under Oiliness Lubricating Conditions, Proc. General Discussion on Lubrication and Lubricants. I. Mech. e, 2 (1937) 223-235.

[26] T. Chen, P. Wei, C. Zhu, P. Zeng, D. Li, R. Parker, H. Liu, Experimental Investigation of Gear Scuffing for Various Tooth Surface Treatments, Tribology Transactions, 66 (2023) 35-46. https://doi.org/10.1080/10402004.2022.2136590

[27] S.-Y. Chern, T.-N. Ta, J.-H. Horng, Y.-S. Wu, Wear and vibration behavior of ZDDP-Containing oil considering scuffing failure, Wear, 478-479 (2021) 203923. https://doi.org/10.1016/j.wear.2021.203923

[28] R.S. Montgomery, Run-in and glaze formation on gray cast iron surfaces, Wear, 14 (1969) 99-105.

[29] M.D. Rogers, Metallographic characterisation of transformation phases on scuffed

cast-iron diesel-engine components：Tribology, , Wear, 14 (1969) 149.

[30] A.A. Torrance, A. Cameron, Surface transformations in scuffing, Wear, 28 (1974) 299-311. https://doi.org/10.1016/0043-1648(74)90187-2

[31] F. Saeidi, A.A. Taylor, B. Meylan, P. Hoffmann, K. Wasmer, Origin of scuffing in grey cast iron-steel tribo-system, Materials & Design, 116 (2017) 622-630. https://doi.org/10.1016/j.matdes.2016.12.044

[32] B. Zhang, X. Ma, L. Liu, Y. Wang, H. Yu, A. Morina, X. Lu, Reciprocating sliding friction behavior and wear state transition mechanism of cylinder liner and piston ring, Wear, (2024) 205293. https://doi.org/10.1016/j.wear.2024.205293

[33] P. Obert, T. Müller, H.J. Füsser, D. Bartel, The influence of oil supply and cylinder liner temperature on friction, wear and scuffing behavior of piston ring cylinder liner contacts - A new model test, Tribology international, 94 (2016) 306-314. https://doi.org/10.1016/j.triboint.2015.08.026

[34] M.S. Shehata, Emissions, performance and cylinder pressure of diesel engine fuelled by biodiesel fuel, Fuel, 112 (2013) 513-522. https://doi.org/10.1016/j.fuel.2013.02.056

[35] F. Saeidi, M. Parlinska-Wojtan, P. Hoffmann, K. Wasmer, Effects of laser surface texturing on the wear and failure mechanism of grey cast iron reciprocating against steel under starved lubrication conditions, Wear, 386-387 (2017) 29-38. https://doi.org/10.1016/j.wear.2017.05.015

[36] C.-h. Yin, Y.-l. Liang, Y. Liang, W. Li, M. Yang, Formation of a self-lubricating layer by oxidation and solid-state amorphization of nano-lamellar microstructures during dry sliding wear tests, Acta Materialia, 166 (2019) 208-220. https://doi.org/10.1016/j.actamat.2018.12.049

[37] C. Li, X. Deng, Z. Wang, Friction behaviour and self-lubricating mechanism of low alloy martensitic steel during reciprocating sliding, Wear, 482-483 (2021) 203972. https://doi.org/10.1016/j.wear.2021.203972

[38] R. Mourhatch, P.B. Aswath, Tribological behavior and nature of tribofilms generated from fluorinated ZDDP in comparison to ZDDP under extreme pressure

conditions—Part 1: Structure and chemistry of tribofilms, Tribology International, 44 (2011) 187-200. https://doi.org/10.1016/j.triboint.2010.10.018

[39] B.F. Zhang, X. Ma, X.Q. Lu, Y. Song, Y.F. Shi, Y.D. Fu, Effect of cylinder liner cast iron microstructure on friction and wear process, Materials Science and Technology. https://doi.org/10.1080/02670836.2022.2130519

[40] R. Ghasemi, L. Elmquist, A study on graphite extrusion phenomenon under the sliding wear response of cast iron using microindentation and microscratch techniques, Wear, 320 (2014) 120-126. https://doi.org/10.1016/j.wear.2014.09.002

[41] E.C. Cutiongco, Y.-W. Chung, Prediction of Scuffing Failure Based on Competitive Kinetics of Oxide Formation and Removal: Application to Lubricated Sliding of AISI 52100 Steel on Steel, Tribology Transactions, 37 (1994) 622-628. https://doi.org/10.1080/10402009408983338